



1 **Measurement report: Effect of wind shear on PM₁₀**
2 **concentration vertical structure in urban boundary layer**
3 **in a complex terrain**

4 Piotr Sekuła^{1,2}, Anita Bokwa³, Jakub Bartyzel¹, Bogdan Bochenek², Łukasz Chmura^{1,2},
5 Michał Gałkowski^{1,4}, Mirosław Zimnoch¹

6
7 ¹ Faculty of Physics and Applied Computer Science, AGH-University of Science and Technology, 19
8 Reymonta St., 30-059 Kraków, Poland

9 ² Institute of Meteorology and Water Management, National Research Institute, Branch of Kraków, 14
10 Piotra Borowego St., 30-215 Kraków, Poland

11 ³ Institute of Geography and Spatial Management, Jagiellonian University, 7 Gronostajowa St., 30-387
12 Kraków, Poland, anita.bokwa@uj.edu.pl

13 ⁴ Max Planck Institute for Biogeochemistry, Department of Biogeochemical Signals, Hans-Knoll-Str. 10,
14 07745 Jena, Germany

15
16 Correspondence to: Anita Bokwa (anita.bokwa@uj.edu.pl)

17
18 **Abstract.** The paper shows wind shear impact on PM₁₀ vertical profiles, in Kraków, southern Poland. The data
19 used consist of background data for two cold seasons (Sep. 2018 to Apr. 2019, and Sep. 2019 to Apr. 2020), and
20 data for several case studies from November 2019 to March 2020. The data is composed of PM₁₀ measurements,
21 model data, and wind speed and direction data. The background model data come from operational forecast results
22 of AROME model. PM₁₀ concentration in the vertical profile was measured with a sightseeing balloon.
23 Significant spatial variability of wind field was found. The case studies represent the conditions with much lower
24 wind speed and a much higher PM₁₀ levels than the seasonal average. The inversions were much more frequent
25 than on average, too. Wind shear turned out to be the most important factor in terms of PM₁₀ vertical profile
26 modification. It is generated due to the relief impact, i.e. the presence of a large valley, blocked on one side with
27 the hills. The analysis of PM₁₀ profiles from all flights allows to distinguish three vertical zones of potential air
28 pollution hazard within the valley (about 100 m deep) and the city of Kraków: 1. up to about 60 m a.g.l. – the zone
29 where during periods of low wind speed, air pollution is potentially the highest and the duration of such high levels
30 is the longest, i.e. the zone with the worst aerosanitary conditions; 2. about 60-100 m a.g.l. – transitional zone
31 where the large decrease of PM₁₀ levels with height is observed; 3. above 100-120 m a.g.l. – the zone where air
32 quality is significantly better than in the zone 1, either due to the increase of the wind speed, or due to the wind
33 direction change and advection of different, clean air masses.

34
35 **1 Introduction**

36 Particulate matter (PM) concentration remains one of the most relevant air-quality concerns in urban
37 environments (Thürkow et al., 2021). Exposure to ambient PM concentration with diameter below 10 µm (PM₁₀)
38 can cause lung irritation, cellular damage, coughing asthma, and cardiovascular diseases (Jeong, 2013). Particles
39 with diameter below 1 µm (i.e. fine and ultrafine particles which constitute in most cases the majority of PM₁₀
40 fraction) have the strongest impact on health because they can reach the deepest portions of the airways or even
41 the blood stream (Franchini and Mannucci, 2007, 2011). Presence of the particulate matter in the ambient air is



42 the result of multiple physio-chemical processes, including local emission, chemical transformation, long-range
43 transport, vertical mixing and deposition, most of which are dependent on meteorological conditions across a large
44 range of spatial and temporal scales (Zhang et al., 2015; Zhou et al., 2020; Thürkow et al., 2021).
45 Local meteorological conditions determine primarily the dispersion of air pollutants, their removal (Trompetter et
46 al., 2013), but they also affect chemical and physical process linked to the origin of the primary and secondary
47 aerosols (Zhou et al., 2020). One of the mostly studied meteorological phenomena is the occurrence of above-
48 ground air temperature gradient inversion, which has a direct impact on the vertical distribution of the
49 concentration of PM₁₀ and its individual components, e.g. black carbon (Zhou et al., 2020) or organic PM₁₀ tracers
50 like levoglucosan (Marynowski et al., 2020). Numerous studies indicate that an important factor that affects the
51 pollution profile is the wind profile (Li and Han, 2016; Zhou et al., 2020), occurrence of low-level jet (Li et al.,
52 2012; Li et al., 2019) or downward flows of pollutants (Han et al., 2018) which may strongly modify diurnal cycle
53 of a pollutant concentration at the lowest part of the troposphere.

54 The vertical structure of the pollutant concentration strongly depends on many factors, including season,
55 meteorological conditions (Wang et al., 2018), topography (Trompetter et al., 2013; Strbova et al., 2017), seasonal
56 variability of local emissions and long-range transport (Li and Han, 2016). Due to this fact it is necessary to
57 continuously study the spatial and vertical distribution of air pollution concentration in urbanized areas to better
58 determine its sources and processes leading to abundant air pollution.

59 Research on the vertical structure of air pollution has been carried out in the past using several methods: stationary
60 point measurements in the profile using the available infrastructure (e.g. Marynowski et al., 2020), balloon flights
61 (e.g. Han et al., 2018; Renard et al., 2020), by airplane or unmanned aerial vehicle (UAV) (Liu et al., 2020),
62 LIDAR (Li and Han, 2016; Wang et al., 2020) or with the use of satellite data (Ferrero et al., 2019). The highest
63 vertical resolution can be achieved with the use of an aircraft (plane, balloon, UAV), however these methods have
64 certain limitations, e.g. lifting capacity, limited flight time and limited maximum reachable altitude, and they
65 cannot operate during unfavorable weather conditions.

66 Throughout the previously published studies focused on the topic of lower-tropospheric air pollution, several types
67 of the pollution concentration vertical profiles can be distinguished:

- 68 - two layers with significantly different concentration, i.e. high concentration in the stratum from the ground level
69 to a certain height, then a transition layer with a rapid decrease in pollutant concentration with height, and a stratum
70 with a low concentration in the profile above; usually linked to thermal inversion occurrence (Strbova et al., 2017;
71 Wang et al., 2018; Samad et al., 2020);
- 72 - a large, constant decrease of a pollutant concentration with height, resulting e.g. from a strong surface emission
73 of a pollutant during stable conditions, or from katabatic flows bringing the pollutants (Strbova et al., 2017), and
74 from removal of the pollutants from upper layers;
- 75 - the occurrence of a layer with increased concentration of air pollution at a certain height, connected to vertical
76 diffusion (Strbova et al., 2017) or diffusion of plumes from elevated sources (Xu et al., 2019);
- 77 - a slight decrease of air pollution with height connected to the occurrence of strong vertical movements (Strbova
78 et al., 2017) or removal of local air pollution due to synoptic processes linked to the advection of air masses.

79 It is noteworthy that many recent studies of air pollution concentration's vertical structure in cities were realized
80 mainly for areas with little variation in the topography (e.g. Paris (Renard et al., 2020), Tianjin (Han et al., 2018)),
81 including coastal areas (Guangzhou (Zhou et al., 2020), Shanghai (Zhang et al., 2017)). In fact, the understanding,



82 and the quantification of pollutant dispersion over complex terrain are much more difficult than over flat areas, as
83 dispersion processes are affected by atmospheric interactions with the orography at different spatial scales
84 (Giovannini et al., 2020). Studies presenting vertical profiles of pollutants' concentration in urbanized valleys are
85 still necessary to better understand impact of meteorology and topography on air pollutant dispersion (Strbova et
86 al., 2017; Zhao et al., 2019; Samad et al., 2020).

87 A key parameter affecting pollutant concentration during the daytime is the height of the atmospheric boundary
88 layer (ABL), which determines the volume of atmosphere available for pollutant dispersion. Turbulent mixing is
89 a key factor which controls the evolution of the ABL depth (Giovannini et al., 2020). One of the important factors
90 is the wind shear as it may essentially modify the structure of mean flow and turbulence in the convective boundary
91 layer (CBL), e.g. by stretching and decoupling of the turbulent structures production or separation of a single-layer
92 CBL into two-layer structure (Fedorovich and Conzemius, 2008; Rodier et al., 2017). Studies presenting the impact
93 of ABL dynamics on vertical pollutant structure indicate that a low-level jet combined with a strong wind shear
94 affect the transportation of the pollution e.g. by removing it (Trompetter et al., 2013) or bringing it in (pushing
95 into the residual layer), and by favoring the growth of ABL height and weakening the stability of the atmosphere
96 (Li et al., 2019).

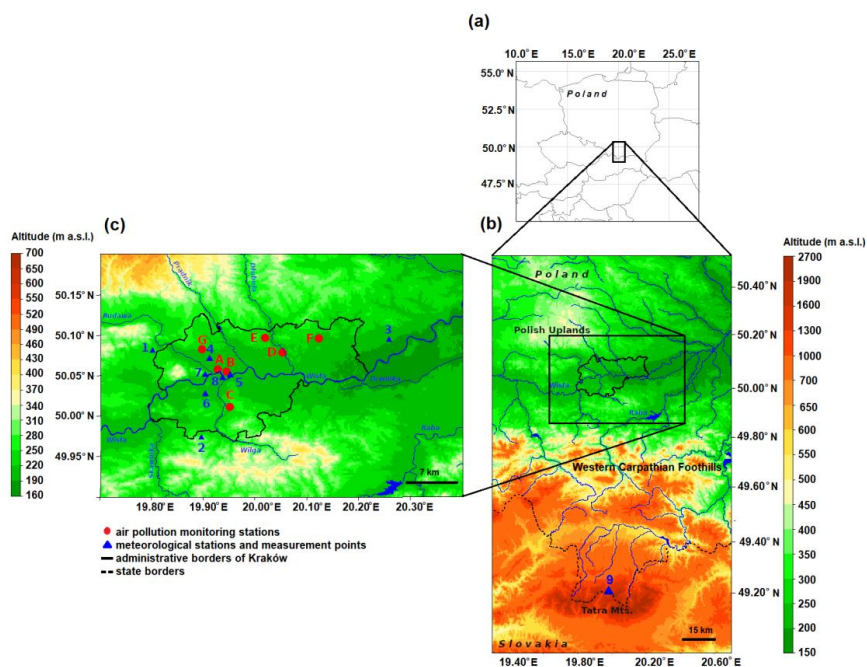
97 The present study is focused on the impact of wind shear on the vertical profile of PM_{10} concentration in Kraków,
98 southern Poland, a city located in a large valley. The properties of ABL, including vertical profile of wind speed
99 and direction, are strongly modified both by the relief and the synoptic situation, and so are the air pollution's
100 dispersion conditions which in turn affects the pollutants concentration's profile. Those circumstances are of the
101 highest importance in a city located in a valley as the built-up areas are located both in the valley bottom as well
102 as on its slopes, i.e. in a vertical profile of the landform. Kraków is a good study area for such considerations as it
103 is located in diversified environmental conditions (described in detail in section 2), and despite various legal
104 actions aimed to reduce local PM_{10} emissions, daily limit values for PM_{10} are still exceeded during cold seasons.
105 Moreover, Kraków is representative for many cities located in Central Europe where aerosanitary conditions are
106 relatively worse in comparison to the cities in the western part of the continent, as presented e.g. in the reports of
107 the European Environment Agency (Air... 2020). Poor air quality is, on one hand, the result of PM_{10} emissions
108 which in the case of Poland are among the highest in Europe (PM_{10} emissions... 2020), however, with a
109 decreasing trend in recent years (Raport... 2017). But high PM_{10} concentrations are also linked to a long-range
110 transport of air pollution from other countries (Godłowska et al. 2015). In the Lesser Poland region (*Małopolska*)
111 where Kraków is located, the main source of PM_{10} is the emission from the municipal and housing sector (78.9%
112 of the annual emission), from transportation (5%), and from industry (7.8%). In Kraków, the emissions related to
113 vehicle traffic account for as much as 12% of annual emission (Raport...2020). Understanding the meteorological
114 processes leading to the enhanced concentration levels is one of the key factors to enable the development
115 strategies for inhabited areas to further reduce the number of smog episodes. To date no studies presenting temporal
116 variability of PM_{10} concentration in vertical profile in cold season has been reported in that region.

117 2 Study area

118 Kraków is a large valley city located in the Wisła River valley, which is parallel to the border of the Carpathian
119 Mts. to the south, and the border of Polish Uplands to the north (Fig. 1). About 100 km south of Kraków, there is
120 the highest ridge of the Carpathians, the Tatra Mts. Kraków is the second largest city of Poland, located in the
121 Lesser Poland region (*Małopolska*), with an area of 326.8 km² and the official number of inhabitants reaching 771



122 thousand (as of Dec. 2018 (Kraków, 2019)). Kraków agglomeration consists of the city itself and highly populated
123 towns and villages which surround it, with the total number of inhabitants is estimated to exceed 1 million. The
124 city's area belongs to three different geographical regions and geological structures, i.e. the Polish Uplands, the
125 Western Carpathians, and the basins of the Carpathian Foredeep in between (Bokwa, 2009). The central part of
126 the city is located in the Wisła River valley, at an altitude of about 200 m a.s.l. In the western part of Kraków, the
127 valley is as narrow as 1 km. However, in the eastern part of the city, the valley widens to about 10 km and there is
128 a system of river terraces. East of the city's borders, the Raba River enters the Wisła River with a valley cutting
129 the Carpathian Foothills from the south to the north. The hilltops bordering the city to the north and the south reach
130 about 100 m above the river valley floor, similar to the hilltops in the western part of the valley which means that
131 the city is located in a semi-concave land form (open only to the east), and sheltered from the prevailing western
132 winds (Fig. 1). The local scale processes linked to the impact of relief include, for example, katabatic flows, cold
133 air pool (CAP) formation, frequent air temperature inversions, much lower wind speed in the valley floor than at
134 the hilltops (e.g. Hess, 1974). According to the studies on thermal stratification obtained for Kraków by using
135 sodar measurements with hourly resolution, in the months from October to March, the mean monthly frequency
136 of stable atmosphere conditions varies from 58.1 % in March to 74.0 % in December (Godłowska, 2019). All
137 factors mentioned above contribute to the poor natural ventilation of the city and the occurrence of high PM_{10}
138 levels, especially in the heating season.
139



140
141
142
143
144

Figure 1. Location of the region studied: a. in Central Europe, b. in southern Poland, c. at the junction of the Wisła River valley, Polish Uplands and the Western Carpathian Foothills.

Explanations: numbers and letters as in table 1 and 2



145 **3 Data and methods**

146

147 **3.1 Surface measurements**

148 The data used consist of background data for two cold seasons (Sep. 2018 to Apr. 2019, and Sep. 2019 to
149 Apr. 2020), and data for several case studies from November 2019 to March 2020. The background data is
150 composed of PM₁₀ measurements from 7 stations, model data, and wind speed and direction data from 4
151 meteorological stations. The data for case studies come from 7 stations with PM₁₀ measurements, model analyses,
152 and 8 meteorological stations (wind speed and direction, air temperature, air humidity and cloudiness) (Fig. 1,
153 Table 1 and 2).

154 Data on PM₁₀ concentrations in Kraków come from data bases of the National Inspectorate of
155 Environmental Protection (NIEP) (<https://powietrze.gios.gov.pl/pjp/archives>). Mean hourly data from 7
156 measurement points were used (Table 1). The measurement points represent several parts of the city, and are
157 located in various types of landform and land use/land cover (see Fig. 1 for the location of the measurement points):

- 158 A. Krasieńskiego St.: street canyon in the city center, in the bottom of the Wisła River valley, with a very
159 busy municipal transportation route and intensive traffic;
- 160 B. Dietla St.: a busy cross-road in the city center, in the bottom of the Wisła River valley, with intensive
161 tram, bus and car traffic;
- 162 C. Kurdwanów district: suburban area with a large district of blocks of flats, in the southern part of the city,
163 about 50 m above the valley floor;
- 164 D. Bulwarowa St.: suburban area with a large district of blocks of flats, located close to the steelworks, in
165 the eastern part of the city, at a terrace of the Wisła River;
- 166 E. Piastów district: suburban area with a large district of blocks of flats, in the eastern part of the city, on the
167 upland slope, about 50 m above the valley floor;
- 168 F. Wadów district: suburban area with agriculture activity and loose residential built-up, located close to the
169 steelworks, at a river terrace in the eastern part of the Wisła valley;
- 170 G. Złoty Róg St.: suburban area with a large district of blocks of flats and residential built-up, on the upland
171 slope, in the western part of the city.

172

173 Table 1. Location of air pollution monitoring stations in Kraków

Symbol	Station	Lat N	Lon E	Altitude (m a.s.l.)	Land form
A	Krasieńskiego St	50.06	19.93	207	Valley bottom
B	Dietla St.	50.05	19.94	209	Valley bottom
C	Kurdwanów district	50.01	19.95	223	Valley slope
D	Bulwarowa St.	50.08	20.05	195	Valley bottom
E	Piastów district	50.10	20.02	239	Valley slope
F	Wadów district	50.10	20.12	218	Valley bottom
G	Złoty Róg St.	50.08	19.90	218	Valley slope

174

175 Background data on wind conditions in the Wisła river valley and the neighboring hilltop were obtained from the
176 stations of the Institute of Meteorology and Water Management – National Research Institute (IMWM-NRI)
177 (Balice, Igołomia and Libertów) and the station of AGH University of Science and Technology (AGH UST),
178 located in the Reymonta St. (city center), on the roof of the Faculty of Physics and Applied Computer Science.



179 Wind speed and direction data of hourly resolution were used. Table 2 and figure 1 show the location of the stations
180 and the range of measurements.

181 3.2 Modelling systems

182 The Aire Limitée Adaptation Dynamique Développement International (ALADIN) system is a numerical
183 weather prediction (NWP) system developed by the international ALADIN consortium for operational weather
184 forecasting and research purposes (Termonia et al., 2018). One of the consortium's development work is to provide
185 several configurations of limited-area model (LAM), which were precisely validated to be used for operational
186 weather forecasting at the 16 partner institutes. These configurations are called the ALADIN canonical model
187 configurations (CMCs). Currently there are three canonical model configurations: 1. ALADIN baseline CMC, 2.
188 Application of Research to Operations at Mesoscale (AROME) CMC, and 3. ALADIN-AROME (ALARO) CMC.
189 AROME CMC and ALARO CMC are operationally used in IMWM-NRI, together with the CY43T2.

190 The background model data come from operational forecast results of AROME model. Operational
191 model AROME CMC 2 km has a horizontal resolution of 2 km x 2 km and 70 vertical levels, the forecast length
192 is 30 h. Size of AROME CMC 2 km domain is 799 x 799 points with centered on geographical point 19.3°E
193 52.3°N. The location of the lowest model level is at 9 m above ground level, and the model top is located at 65 km
194 above ground level. During the analyzed periods model version has been changed from CY40T1 to CY43T2 (11
195 Feb. 2020). Seasonal verification of the AROME CMC model forecast results showed compliance new version
196 with the previous one (Bochenek et al., 2020).

197 ALARO model was used to prepare lateral boundary data for AROME model. ALARO CMC CY43T2
198 is a non-hydrostatic model, with a horizontal resolution of 4 x 4 km and 70 vertical levels. The model configuration
199 ALARO CMC and AROME CMC has been validated by the ALADIN team at IMWM-NRI for CY43T2 for
200 resolution 4 km x 4 km and 2 km x 2 km, respectively.

201 Archival forecasts of the AROME CMC model with temporal resolution of 1h (forecast hours from 6th
202 to 29th), were used to study the characteristics of vertical wind and temperature profiles in the valley, with special
203 focus on 3 height levels (50, 100 and 200 m a.g.l.), as the valley depth is about 100 m. Analyses were conducted
204 at 4 selected points, representing Balice meteorological station, TV tower with vertical profile measurements, city
205 center, and Bulwarowa St. (PM₁₀ measurements). The points mentioned are located along the valley bottom in the
206 W-E cross section.

207 3.3 Vertical profile observations and data verification

208 For the period from November 2019 to March 2020, additional data for the case studies are available.
209 They consist of measurements of PM₁₀ concentration in the vertical profile, performed on 31 days selected. The
210 PM₁₀ profiles' measurements were carried out in cooperation with the company Balon Widokowy sp. z o. o.
211 (<http://balonwidokowy.pl/>) which operates commercially the sightseeing balloon in Kraków. The PM₁₀
212 measurements were conducted up to maximum altitude of almost 300 m a.g.l. Balloon flights were performed in
213 the western part of the city, at the Wisła River, in the city center, close to the air quality monitoring stations
214 Krasieńskiego St. and Dietla St.

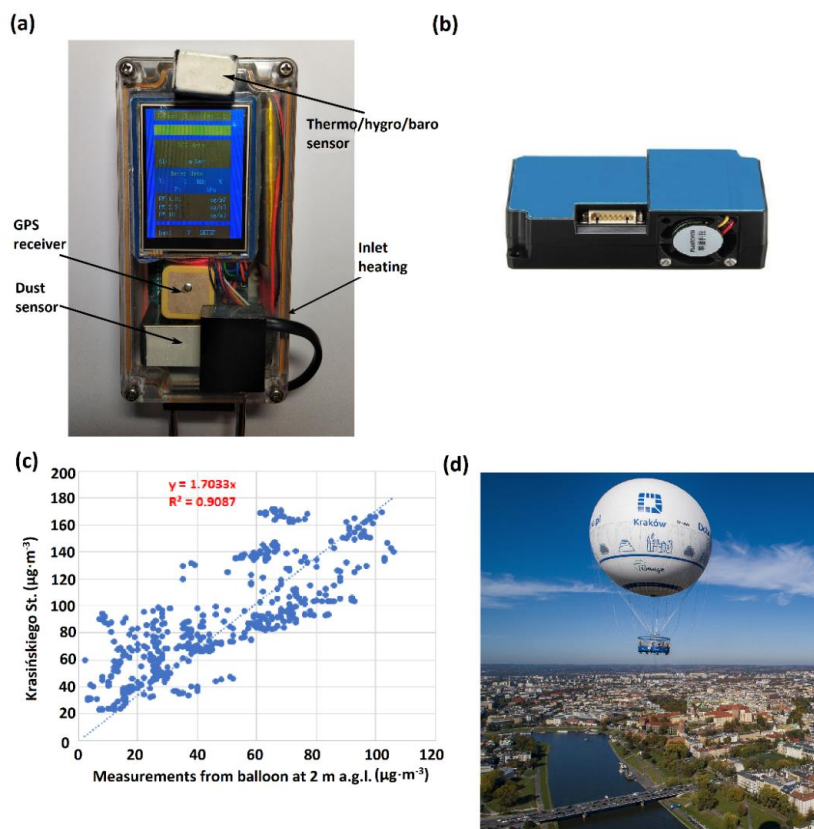
215 Measurements of PM₁₀ concentration in the vertical profile were conducted by Personal Dust Monitor (PoDust
216 v1.1) system based on low-cost Plantower PMS1003 optical dust sensor and Arduino platform presented on Figure
217 2. The measurement system was attached to outside of the balloon basket. It was build based on the Arduino Mega
218 2560 microcontroller, responsible for communication with the sensors, storing the measurements with 1 second



219 resolution on the memory card, and sending information in real time to the database using WiFi connection. To
220 reduce the impact of water vapor on PM₁₀ measurement during the fog conditions, sensor inlet was heated up to
221 60°C. To provide information on an actual location and other environmental conditions, the system was equipped
222 with a GPS receiver and thermo/hygro/baro sensor providing e.g. the altitude estimated with combined GPS and
223 barometer signals.

224 The measurement campaign covered the period from November 28, 2019, to March 3, 2020, during which 317
225 flights were conducted (31 days, 634 vertical profiles). Maximum flight altitude varied between 78 and 284 m
226 a.g.l., depending on vertical wind profile and number of passengers. Typical flight altitude during sightseeing
227 flight was 150 m a.g.l., but during low wind speed at higher altitudes and low passenger load, the maximum altitude
228 was increased. The measurements were performed at different hours. The balloon's flight speed does not exceed 1
229 m·s⁻¹ (ascent up to 0.8 m·s⁻¹, descent approximately up to 0.6 m·s⁻¹), flight time (ascent/descent) depended on the
230 maximum altitude and ranged from 2-3 minutes (for maximum height 100 m a.g.l.) up to 6-10 minutes (for
231 maximum height 300 m a.g.l.).

232 The frequency of flights depended on meteorological conditions and the number of customers. More than 70% of
233 the flights were performed up to 180 m above ground level, flights reaching over 200 m above ground level made
234 only 15% of cases. Almost 50% of vertical profiles were conducted between 12 and 15 UTC, while profiles from
235 15 to 20 UTC constitute 23% of cases. The flight altitude depended on the wind speed in the whole vertical profile
236 of the balloon range, which was measured directly during the flight. Figure 2 presents comparison of PM₁₀
237 measurements from balloon device, conducted at 2 m a.g.l., and measurements from the nearby Krasieńskiego
238 station. As the measurements from Krasieńskiego station are of hourly resolution, linear interpolation of two
239 adjacent measurements was applied to obtain the same data resolution as for the balloon. The intersection point of
240 the straight line matching the graph has been set to 0 because tests on the Plantower sensor have shown the correct
241 measurement for a concentration close to 0 µg·m⁻³.



242

243 *Figure 2. Self-designed and built air pollution measuring system (a), low cost sensor Plantower PMS1003 PM*
244 *component (b), correlation of measurements from balloon location and closest air pollution station (Krasinskiego*
245 *St.) with fitted regression curve and R squared factor (c) and (d) sightseeing balloon (source:*
246 *<http://balonwidokowy.pl>).*
247

248 Data on meteorological conditions, in synoptic and local scale, for Kraków for days with balloon flights, were
249 obtained from the meteorological stations already mentioned above, and additionally from two stations
250 administered by the Jagiellonian University (JU) (Campus JU, Botanical Gardens) and one station administered
251 by IMWM-NRI (Kasprowy Wierch Mt., in the Tatra Mts.). The JU also administers measurements at the television
252 tower (the technical details can be found in Bokwa A. 2010); the tower belongs to Emitel company.

253 Due to possible effect of foehn occurrence on ABL modification, potential foehn occurrence was determined
254 based on the criteria of Ustrnul (1992), upon the analysis of the measurement data from the synoptic stations
255 Kasprowy Wierch Mt. (wind speed and direction) and Balice (wind speed and direction, and air humidity). One of
256 the criteria determining foehn occurrence in Kraków is the presence of *Alto cumulus lenticularis* clouds (*Ac len*)
257 which are one of the effects of mountain waves. Information about *Ac len* clouds occurrence was obtained from
258 the station in the Botanical Gardens in Krakow. Data on air temperature in the vertical profile of the Wisła river
259 valley were obtained from stationary measurements at the altitudes 2, 50 and 100 m a.g.l., from TV tower located



260 in the western part of the valley. Table 2 and figure 1 show the location of the stations and the range of
261 measurements.

262 *Table 2. Location of meteorological stations in Kraków and its vicinities, station Kasprowy Wierch, balloon*
263 *measurement point and meteorological elements used in the study.*

No.	Station	Lat N	Lon E	Altitude (m a.s.l.)	Manager of the station	Land form	Elements Used
1	Balice	50.08	19.80	237	IMWM-NRI	Valley bottom	V, D, T, RH
2	Libertów	49.97	19.90	314	IMWM-NRI	Hill top	V, D, T, RH
3	Igołomia	50.09	20.26	202	IMWM-NRI	Valley bottom	V, D, T, RH
4	Reymonta St.	50.07	19.91	220	AGH UST	Valley bottom	V, D, T, RH
5	Botanical Gardens	50.05	19.95	206	JU	Valley bottom	V, D, Ac len clouds
6	Campus JU	50.03	19.90	233	JU	Valley bottom	V, D
7	TV Tower: 2 m a.g.l.	50.05	19.90	222	JU	Valley bottom	T, RH
	50 m a.g.l.						
	100 m a.g.l.						
8	Balloon measurement point	50.05	19.94	200	AGH UST	Valley bottom	PM10
9	Kasprowy Wierch	49.23	19.98	1998	IMWM-NRI	Mountain peak	V, D, T, RH

264 Explanations: AGH UST – AGH University of Science and Technology, JU – Jagiellonian University.
265 More information about the measurement points administered by JU can be found in Bokwa (2010). V –
266 wind speed, D – wind direction, T – air temperature, RH – relative humidity
267

268 For the analysis of case studies data, a different model configuration was used than for background data from the
269 two cold seasons. Nonoperational configuration of the AROME CMC 1 km x 1 km CY43T2 (AROME CMC 1
270 km) was applied. Operational model ALARO CY43T2 was used to prepare lateral boundary data for AROME
271 model version CY43T2. Non-hydrostatic model AROME CMC 1 km has a horizontal resolution of 1 km x 1 km
272 and 87 vertical levels, the forecast length was 30 h. Size of AROME CMC 1 km domain was 810 x 810 points
273 with centered on geographical point 20°E 50°N. The location of the lowest model level is at 9 m above ground
274 level, and the model top is located at 50 km above ground level. Details concerning the height of the lowest model
275 levels up to 3 km altitude, information about parametrization schemes used in AROME model and topographic
276 map of model domain are included in table A1, A2 and fig. A1. The data obtained with the model were used to
277 provide vertical profiles of wind speed and direction, air temperature, relative humidity and Turbulent Kinetic
278 Energy (TKE) with 1-hour temporal resolution, in the points representative for a western, central and eastern part
279 of the city, corresponding to the measurements in Balice, Bulwarowa St. and balloon measurement point
280 respectively. Additionally, N-S cross-sections through the valley at those points were obtained for the same
281 elements. For selected cases, wind, TKE and air temperature fields at selected levels were obtained for the whole
282 area of Kraków and its surroundings.



283 Verification of forecast results of AROME CMC 1km was performed for 24-h periods (i.e., from 6th to 29th hour
284 of forecast with 1-hour resolution) for selected 31 days of the case study period. Data obtained from 4
285 meteorological stations (Balice, Libertów, Igołomia and Reymonta St.) were used to verify the model forecast of
286 air temperature, air humidity and wind components in the valley bottom and at the hill top. The value of root mean
287 square error (RMSE) between observation and forecast were lower than 2°C for air temperature, 1.5 m·s⁻¹ for wind
288 speed and 14% for relative humidity at all meteorological stations. Air temperature and humidity measurements
289 at 50 and 100 m a.g.l. from TV tower station were used to verify model forecast of atmosphere stratification in the
290 west part of the Wisła River valley. Values of RMSE and difference (bias) for air temperature and humidity for
291 both altitudes (i.e. 50 and 100 m) are similar, on average RMSE was equal 1.5°C for air temperature and 9.5% for
292 relative humidity.

293 Data analysis for background period (i.e. two cold seasons) included calculation of standard characteristics for
294 particular elements studied, in order to: 1. determine their spatial variability in the study area; 2. define wind shear
295 conditions; and 3. in order to be used further for the verification of the representativeness of the case study period.
296 The indices used included wind roses for the ground stations, wind speed histograms for three levels (50, 100 and
297 200 m a.g.l.), air temperature gradients, differences in PM₁₀ concentrations between the stations, and the
298 correlation between PM₁₀ concentrations and wind speed.

299 For the case study period, first the PM₁₀ concentration vertical profiles were classified with a subjective method of
300 fitting the linear curve to each vertical profile. Based on R squared coefficient, the angle of the straight line and
301 residual values classification has been made. Each profile was checked manually whether it was correctly assigned
302 to a given group. For this purpose, neighboring flights on a given day were analyzed, too. Objective classification
303 methods could not be used due to differences in flight heights and the PM₁₀ measurement altitudes in particular
304 flights. Three groups/patterns of PM₁₀ concentration vertical profiles were obtained, and for each of them all
305 meteorological data were analyzed in order to determine their significance in controlling the air pollution vertical
306 structure.

307 **4 Results**

308 **4.1 Spatial and temporal variability of anemological conditions**

309 Analysis of the data on wind speed and direction from three meteorological stations in the Wisła valley (Balice,
310 Reymonta St., Igołomia) and one station in the nearby hilltop (Libertów) for the two cold seasons (Sep. 2018 to
311 Apr. 2019 and from Sep. 2019 to Apr. 2020) indicated significant spatial variability of that element due to the
312 complexity of the landforms and the presence of urban structures. However, the differences of the wind structure
313 between the both seasons were negligible. In terms of spatial variability, the average frequency of weak wind (up
314 to 2 m·s⁻¹) varied from 43% in Balice to 61% in Reymonta St.; in Libertów and Igołomia the values reached 50%
315 and 53%, respectively. For the wind speed ≥ 4 m·s⁻¹, the highest average frequency was measured in Balice (27%),
316 while in Libertów and Reymonta St. it did not exceed 10%, and in Igołomia reached 21%. Wind speed ≥ 10 m·s⁻¹,
317 was noted in Igołomia and Balice only. Dominant wind directions are strongly linked to the relief impact. In Balice
318 those are SW and NE, in Igołomia and Reymonta St. W and E, while in Libertów it is the western sector: SW to
319 WNW (Fig. A2).



320 Similar calculations were also performed for the case studies period, i.e. 31 days during which the flights were
321 conducted, within the period from November 28, 2019 to March 3, 2020, in order to check whether these results
322 can be treated as representative for the whole cold period. The frequency of wind speed $\leq 2 \text{ m}\cdot\text{s}^{-1}$ was much larger
323 than the average value for both seasons: from 62% in Balice to 83% in Reymonta St., while the frequency of wind
324 speed $\geq 4 \text{ m}\cdot\text{s}^{-1}$ was much smaller: from 0.1% in Reymonta St. to 7.9% in Balice. Dominant wind directions for
325 the case study period did not differ significantly from the average values for both seasons. Therefore, the case
326 studies period can be considered as representing days with very low wind speed at the station level.

327 On the basis of archival forecasts of the AROME operational model, the characteristics of vertical wind profiles
328 in the valley for four points located in the valley bottom in a W-E cross-section (i.e. Balice, TV tower, city center,
329 Bulwarowa St.), for the two seasons, were examined at three levels: 50, 100 and 200 m a.g.l. and for every hour
330 of the day. The analysis did not show significant differences between the seasons. For nearly 50% of the cases, the
331 velocity at 50 m a.g.l. in the valley did not exceed $4 \text{ m}\cdot\text{s}^{-1}$. Wind speed at levels 100 and 200 m a.g.l. did not exceed
332 $10 \text{ m}\cdot\text{s}^{-1}$ and $12 \text{ m}\cdot\text{s}^{-1}$ for more than 90% of cases, respectively.

333 Wind direction forecasts at the three levels were used to analyze the frequency of significant wind direction change
334 in the vertical profile (wind shear), between levels 50 and 100 m a.g.l., 100 and 200 m a.g.l. and 50 and 200 m
335 a.g.l. Minimum value of significant wind direction change was set to 20° , on the basis of analyses. Wind direction
336 studies were performed for diurnal (i.e. 6 to 17 UTC) and nocturnal (i.e. 18 to 5 UTC) periods. For the point
337 representing city center, and located close to the balloon sounding site, for both cold seasons, the percentage of
338 large wind direction changes which lasted more than 4 hours (between levels 50 and 200 m a.g.l.) equaled 9.5%
339 and 31.9% during daytime and nighttime, respectively. The values for the case study period reached 42% and 52%,
340 and for the changes which lasted over 4 hours it was 23.7% and 46.2%.

341 On the basis of the above comparisons, it is possible to conclude that on the days which belong to the case study
342 period, wind speed was much lower than on average during both cold seasons, while large wind direction changes
343 were much more frequent.

344 4.2 Spatial and temporal PM₁₀ concentrations' variability

345 The analysis of data on PM₁₀ concentration from all monitoring points operated by NIEP and described in section
346 3, from both cold periods analyzed, was performed in order to determine to what extent the measurements of the
347 PM₁₀ vertical profile realized close to the city center, in the western, narrow part of the valley, are representative
348 for other city's areas. First, significant difference were found between both of the analysed cold seasons; in the
349 season 2019-2020, the mean concentrations were lower than in the previous cold season at all stations, except
350 Bulwarowa St. The number of days with mean daily concentration $\leq 50 \mu\text{g}\cdot\text{m}^{-3}$ increased by as much as 15% in
351 Kurdwanów dist. and Dietla St., with a simultaneous decrease in the number of days with mean daily concentration
352 50-100 (-10% on Kurdwanów dist. and -8% on Dietla St.). The number of days with an average daily concentration
353 $\geq 50 \mu\text{g}\cdot\text{m}^{-3}$ in the season 2019-2020 ranged between 35 and 63 for most of the stations except the Krasieńskiego
354 St., located close to the balloon site, where the number of such days was equal to 101. In the season 2019-2020,
355 days with mean daily concentration of 100-150 $\mu\text{g}\cdot\text{m}^{-3}$ occurred at four stations only: Krasieńskiego St.: 14 days,
356 Bulwarowa St.: 7 days, Kurdwanów dist.: 4 days, Złoty Róg St.: 3 days, while in 2018-2019, such high
357 concentrations occurred almost at the same stations, but the numbers were significantly higher, e.g. 28 days in



358 Krasińskiego St., and from 12 to 14 days in Złoty Róg St., Dietla St., and Kurdwanów dist. Maximum PM₁₀
359 hourly concentration reached 378 $\mu\text{g}\cdot\text{m}^{-3}$ in Dietla St. on 18.02.2019. Therefore, it can be stated that the western
360 part of the city, located in the narrow part of the valley floor, experiences much worse air pollution concerning
361 PM₁₀ than the eastern part, located in the wide part of the valley. The vertical PM₁₀ measurements can be then
362 considered representative for the western part of the valley.

363 As weak winds prevailed during the case study periods, hourly PM₁₀ concentrations were analysed for particular
364 wind speed ranges, and wind measurements from Reymonta St. were used (i.e. representative for the western part
365 of the city). Concerning high PM₁₀ levels, which are the most dangerous for human health, the percentage of the
366 cases with wind speeds below 1 $\text{m}\cdot\text{s}^{-1}$ (during the both cold seasons) when the concentration was higher than 100
367 $\mu\text{g}\cdot\text{m}^{-3}$ varied from 7.3% (Wadów dist.), 10-11% (Dietla St., Bulwarowa St. and Piastów dist.) 13.6% at Złoty Róg
368 St., to 15.3% at Kurdwanów dist. and 25.7% at Krasińskiego St. For cases $\geq 150 \mu\text{g}\cdot\text{m}^{-3}$, the values varied from
369 0.7-0.8% (Bulwarowa St., Piastów and Wadów dist.), 1.6% at Dietla St., 1.9% at Złoty Róg St., to 4.1% at
370 Kurdwanów dist. and 5.7% at Krasińskiego St. The data shows large differences in PM₁₀ horizontal distribution
371 within the city, and a relatively high frequency of PM₁₀ dangerous concentrations, as high as double the allowed
372 mean daily level.

373 Figure A3 shows the correlation between PM₁₀ concentrations at individual air pollution stations and the wind
374 speed at Reymonta St. The logarithmic curves were fitted to the data.

375 Due to the fact that PM₁₀ levels differ significantly between the two cold periods analyzed (i.e. 2018-2019 and
376 2019-2020), PM₁₀ data for the case studies period were compared with the data for the whole season 2019-2020
377 only, in order to check their representativeness for the season. During the case studies period, hourly PM₁₀
378 concentrations $\leq 50 \mu\text{g}\cdot\text{m}^{-3}$ reached from 23% for Krasińskiego St. to 50-60% for the Dietla St., Piastów and
379 Wadów districts, while during the whole cold season 2019-2020 they were much more frequent and varied from
380 57% for Krasińskiego St. to over 80% for Dietla St., Piastów and Wadów districts. Parallel, values $\geq 150 \mu\text{g}\cdot\text{m}^{-3}$
381 for most of the stations were up to 3% (with a minimum in Dietla St. 0.4%) but in Krasińskiego St. they reached
382 7%, while for the whole season the highest value was 1.3%. That means that the case studies represent not only
383 the conditions with much lower wind speed than the seasonal average but also the conditions with a much higher
384 PM₁₀ levels than on average.

385 4.3 Vertical air temperature gradient

386 Based on the high-resolution forecasts of the AROME CMC 1 km model, an analysis of the vertical temperature
387 gradient between the model level 50 and 220 m a.g.l. for the city center, for the case studies period, against the
388 background data from two cold seasons, has been performed. The presence of a thermal inversion is an important
389 factor which limits the PM₁₀ dispersion conditions, and therefore contributes to its high levels. The gradient values
390 were calculated separately for the daytime (6-17 UTC) and nighttime (18-5 UTC), as the phenomenon is usually
391 much more frequent during the nighttime than daytime. The frequency of a gradient greater than 0.5°C/100 m (i.e.
392 thermal inversion) in the night time was rather similar in the case study period (48%) and in the cold seasons
393 (38%), while during the daytime, the value for case study period was much larger than for both seasons (32% and
394 7%, respectively). It means that during the study period, the inversions were much more frequent than on average
395 in the cold season which contributed to the much higher PM₁₀ concentrations, mentioned above.



396 The frequency of thermal inversion is linked to wind speed (Table A3). An analysis of the temperature gradient
397 versus wind speed at 50 m a.g.l. was performed for the both cold seasons, jointly. The studies indicated that for
398 wind speed $< 2\text{m}\cdot\text{s}^{-1}$ the frequency of the gradient greater than $0.5^\circ\text{C}/100\text{ m}$ was 45%, and for wind speed $2\text{--}4\text{ m}\cdot\text{s}^{-1}$
399 it decreased to 31% of cases. High PM₁₀ concentrations in the study period were then the effect of joint impact
400 of low wind speed and thermal inversion, generated by the city location in the concave landform.

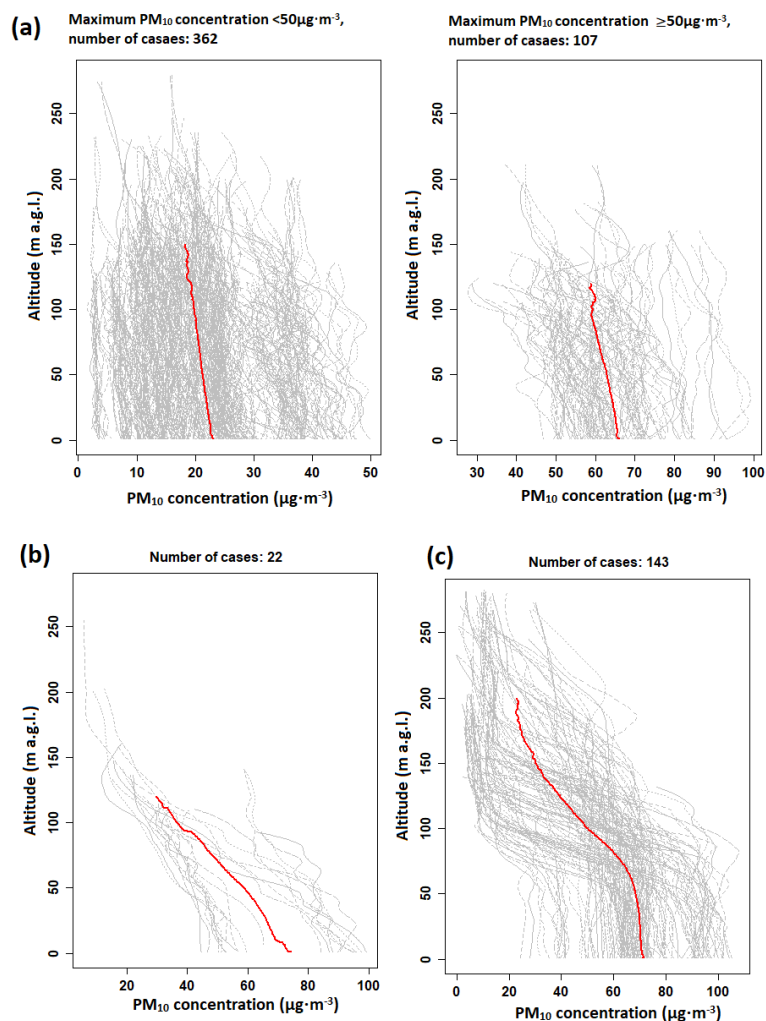
401 **4.4 Vertical profiles of PM₁₀ concentration**

402 There were three types of PM₁₀ vertical profiles distinguished (Fig. 3):

- 403 • Type I – almost constant value of PM₁₀ concentration in the vertical profile (small fluctuations, weak
404 decrease);
- 405 • Type II – strong decrease of PM₁₀ concentration in the vertical profile;
- 406 • Type III - the occurrence of three layers of PM₁₀ concentration: 1. constant concentration in the lower
407 part of the profile, 2. transition layer above, and 3. the upper layer where a sudden drop of PM₁₀
408 concentration is observed.

409

410 Out of 31 analyzed days, type I was observed on 26 days, type II on 7 days and type III on 13 days. For 11 out of
411 31 days, 2 types of profiles were observed on 11 days, and all 3 types on 4 days (Table A4). Occurrence of different
412 profile types during a single day indicates significant fluctuations of meteorological conditions.



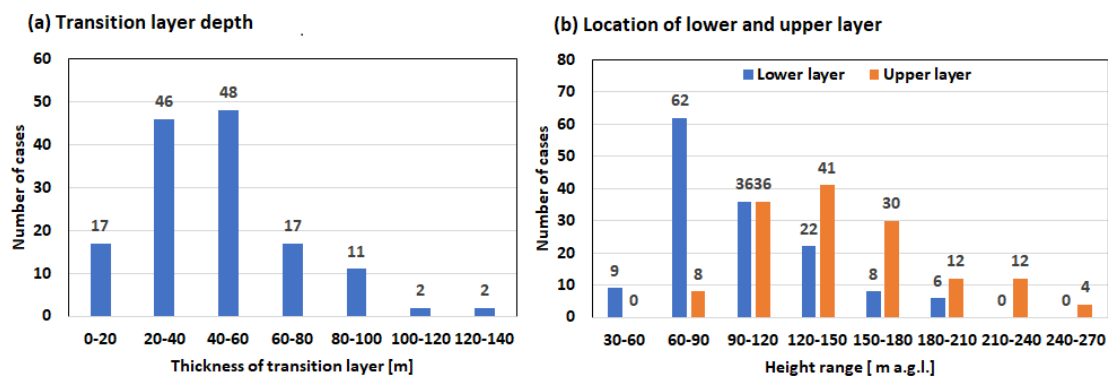
413
414 *Figure 3. Classification of PM₁₀ vertical profiles into the three main types: a. type I (it is presented in two plots*
415 *due to a wide range of PM₁₀ concentration values); b. type II; c. type III*
416 *Explanations: gray lines – individual vertical profiles of PM₁₀ concentration, red lines - mean profiles of a certain*
417 *type*
418

419 Vertical profiles assigned to type III differ a lot in the position and thickness of the transition layer. The dominant
420 pattern in figure 3c is characterized by a sudden drop in pollution at the valley top which is about 100 m a.g.l. The
421 transition layer was further determined with the features presented below:

- 422 1. Calculation of mean concentration in the lower layer (up to 70 m above the ground level) and upper layer
423 (the last 20 m in profile)
- 424 2. Determination of the altitude at which the decrease of PM₁₀ concentration in the lower layer is ≥ 15 µg·m⁻³
425 ³ between two neighbor measurement levels; for the upper layer the difference was set ≥ 5 µg·m⁻³. In case
426 of the occurrence of the transition layer only (i.e. no upper layer), the last point of the profile was
427 considered the upper level of the transition layer.



428 3. Each flight was checked whether it was necessary to manually modify the height of the layers on the basis
429 of the analysis of the entire profile, and such correction was made for 37 out of 143 profiles.
430 Figure 4 presents characteristics of transition layer for all selected vertical profiles.



431
432 *Figure 4. Characteristics of the transition layer in the vertical profiles of PM₁₀ concentrations in type 3.*

433

434 It should be noted that the vertical profiles in type I, could have been the lower part of profiles of type III; the low
435 flight maximum altitude, associated with the occurrence of a strong wind, did not allow to continue the
436 measurements higher and verify the hypothesis.

437 4.5 Impact of relief and meteorological conditions on PM₁₀ concentrations vertical profiles

438 Type I

439 On 18 out of 26 days analyzed, mechanical and thermal turbulence led to strong convection. However, the effect
440 of mechanical turbulence was a quick increase of convection layer thickness during the day, followed with its
441 sudden decrease in the evening, while thermal turbulence caused gradual development of the convection layer and
442 its lower thickness. The upper limit of the convection layer was defined with the application of TKE profiles and
443 reached 300-500 m a.g.l. The flights height on those days did not exceed those values which was the reason of the
444 almost constant PM₁₀ concentration observed.

445 On 5 out of 26 days analyzed, convection layer was controlled by the thermal turbulence. Its thickness did not
446 exceed 200 m a.g.l., and wind shear was observed above but the flights reached only 150 m a.g.l. Therefore, the
447 upper layer with – most probably – much lower PM₁₀ concentrations could not be observed. Such scenario is an
448 example of a modification of the turbulence at the top of CBL, i.e. a reduction of vertical mixing efficiency by
449 wind shear, presented e.g. in Rodier et al., 2017.

450

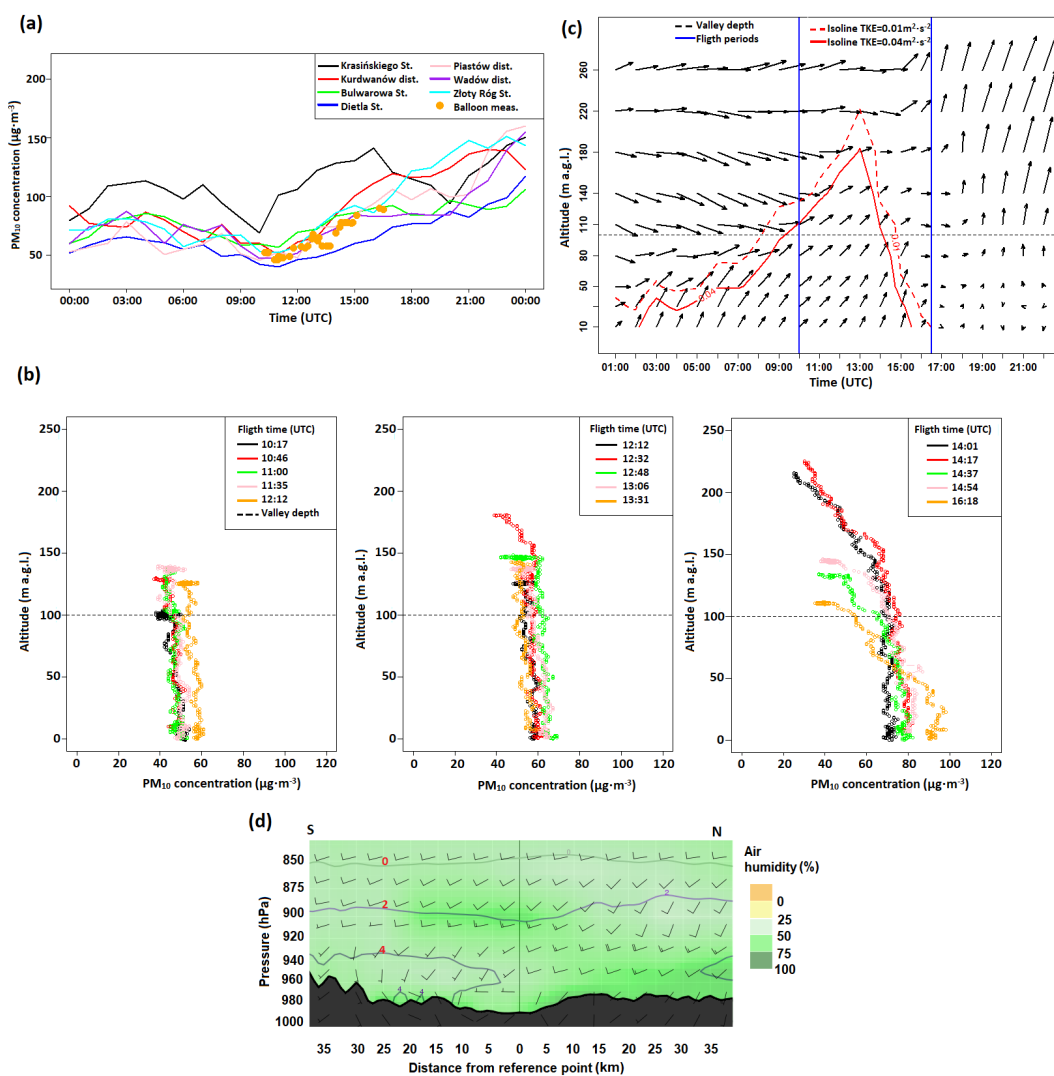
451 Type II

452 The sudden decrease of PM₁₀ concentration with height in profile type II was an effect of two processes: an increase
453 of pollutants emission near the ground and removal of the pollution from the upper layers. The latter was due to
454 mechanical turbulence caused by the presence of the wind shear. The wind shear was the effect of an increase of



455 wind speed close to the valley top and significant wind direction change caused by the complex topography impact.
456 Sudden decrease of PM_{10} concentration at 6 out of 7 days was observed at evening hours, after weakening of
457 convection movements and wind speed close to the ground. During 2 out of 7 days selected, the occurrence of
458 turbulence was caused by the presence of mountain waves which strongly modified convection movements. The
459 analysis of the flights showed that it was a short-time phenomenon which can occur during e.g. a momentary lack
460 of convective movements or a passage of an atmospheric front.

461 The case study of 27 Jan., 2020, is presented below as an example of the processes described above. In the early
462 morning hours until 9 UTC, there was a humid cold pool in the valley, drier and warmer air moved over the valley
463 from the west. Between 6 and 12 UTC, there was a gradual break of the inversion and a decrease in humidity in
464 the profile observed at 50 and 100 m a.g.l. at the tower station. Until 12.00 UTC, the PM_{10} concentration at the
465 ground stations did not change significantly, after 12 UTC an increase of PM_{10} concentration was visible in the
466 vertical profile. The increased concentration of PM_{10} at Krasieńskiego St. compared to other stations maintained
467 until 17 UTC. The difference in concentration between the ground-level measurement from the balloon point and
468 Krasieńskiego St. was in the range of $50\text{--}70 \mu\text{g}\cdot\text{m}^{-3}$ for most of the time. Vertical profiles of TKE indicated that
469 convection layer during this day reached up to 200–220 m a.g.l., isolines of TKE equal $0.01 \text{ m}^2\cdot\text{s}^{-2}$ and $0.04 \text{ m}^2\cdot\text{s}^{-2}$
470 are presented at Figure 5c. Flights between 10 and 14 UTC indicated a constant PM_{10} concentration value in the
471 profile up to 150 m a.g.l. Linear decrease of PM_{10} concentration above 150 m a.g.l. was noticed at higher flights
472 around 12:30 UTC and 14:00–14:30 UTC. The consequence of the disappearance of convection layer (which began
473 at 13 UTC) and mechanical pollution removal from the layers above the valley was visible at flights after 14:30
474 UTC. The strongest decrease in the concentration in the vertical profile was observed during the last flight; the
475 height of ground layer with stable PM_{10} concentration did not exceed mean height of the buildings in the city (30
476 m a.g.l.), and above this layer there was a linear decrease in PM_{10} concentration. The decrease in concentration in
477 the layer up to 150 m a.g.l. was related to the occurrence of a wind direction change from SW to W (see the cross
478 section at 16 UTC in fig. 5 d); above this layer, a linear increase in wind speed occurred (see wind profiles in fig.
479 5 c). During the night, there was a separation of the valley wind and topographically channeled airflow, i.e. the
480 wind in the valley weakened, and at the valley top the wind speed increased.



481

482 *Figure 5. Hourly concentration of PM₁₀ at air pollution stations on 27 Jan., 2020: a) ground-level measurements*
 483 *during balloon soundings, b) vertical profiles of PM₁₀ concentration, c) wind profile forecast with added isolines*
 484 *of TKE equal 0.01 m² s⁻² and 0.04 m² s⁻² for point representing city center. Measurement period is marked with*
 485 *blue vertical lines. (d) Air temperature (contour lines), air humidity (background colour) and wind speed (in knots)*
 486 *and direction (graphical symbols) in the SW-NE cross section through Kraków and its vicinities at 16 UTC for the*
 487 *sounding location.*

488 Explanation: valley depth is the altitude of the hilltops surrounding the valley marked at 100 m a.g.l. with a dashed line in
 489 fig. b and c

490

491

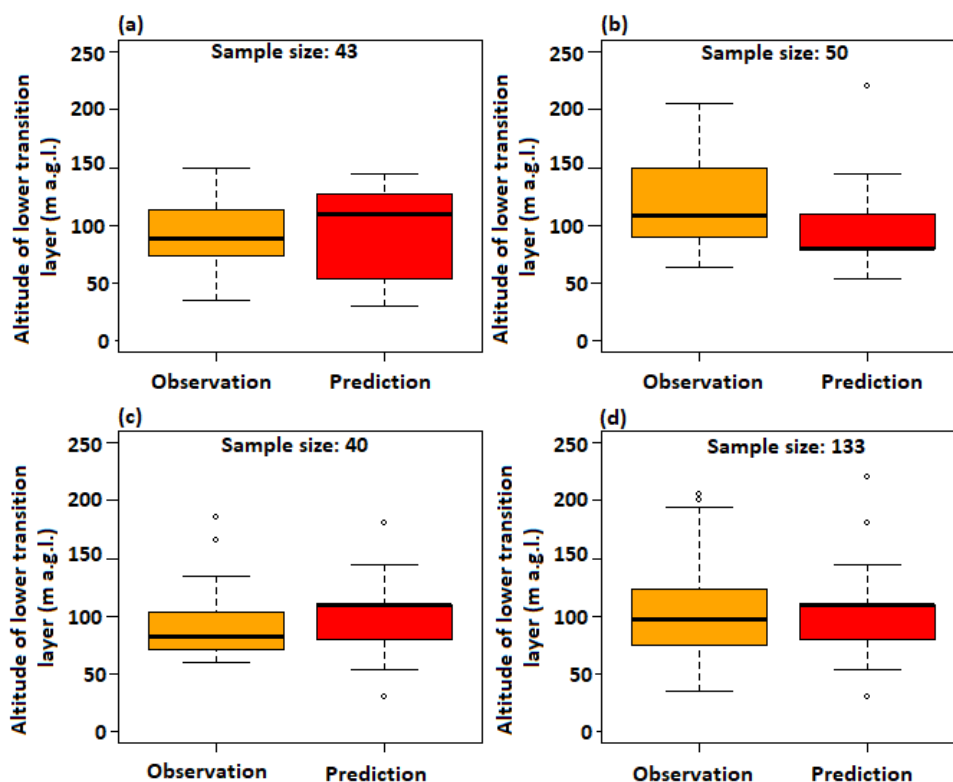
492



493 Type III

494 Type III of PM₁₀ concentration vertical profile was found on more than 40% of measurement days (13
495 out of 31 days). The vertical wind profiles indicated that during the most of selected days a significant wind
496 direction change (wind shear) was observed close to the valley top (i.e. about 100 m a.g.l.) or at upper layers. Wind
497 shear occurred either in a thin layer (i.e. as a sudden change between two neighboring vertical model levels, in a
498 layer up to 50 m thick), or in a thick layer (100-200 m). The occurrence of the wind shear was also accompanied
499 by an increase in wind speed, which was responsible for pollution removal from the upper layer. Wind direction
500 observed at the lower layer was determined by the local topography (valley wind), whereas at upper layer there
501 was regional topographically channeled airflow. The separation of the two atmospheric layers by a strong wind
502 shear for selected cases was reinforced by the advection of warmer air (on 8 days out of 13 analyzed). In case of a
503 cold pool occurrence in the valley, the vertical transport of air pollution was hindered by the thermal inversion
504 intensification. The analysis of TKE vertical profiles and wind speed showed that the height of the transition layer
505 depends on the height of the convection layer and the occurrence of wind shear (Fig. 6). The wind shear occurrence
506 was defined as a wind direction change between two neighbor vertical model levels, and the minimum value was
507 set to 20 deg. If the predicted height of convection layer and wind shear occurrence occurred at the same model
508 level, wind shear was connected to jet stream absence which was modifying convection layer. It was observed for
509 20 flights, on 6 days of 13 analyzed (Fig. 6c).

510



511

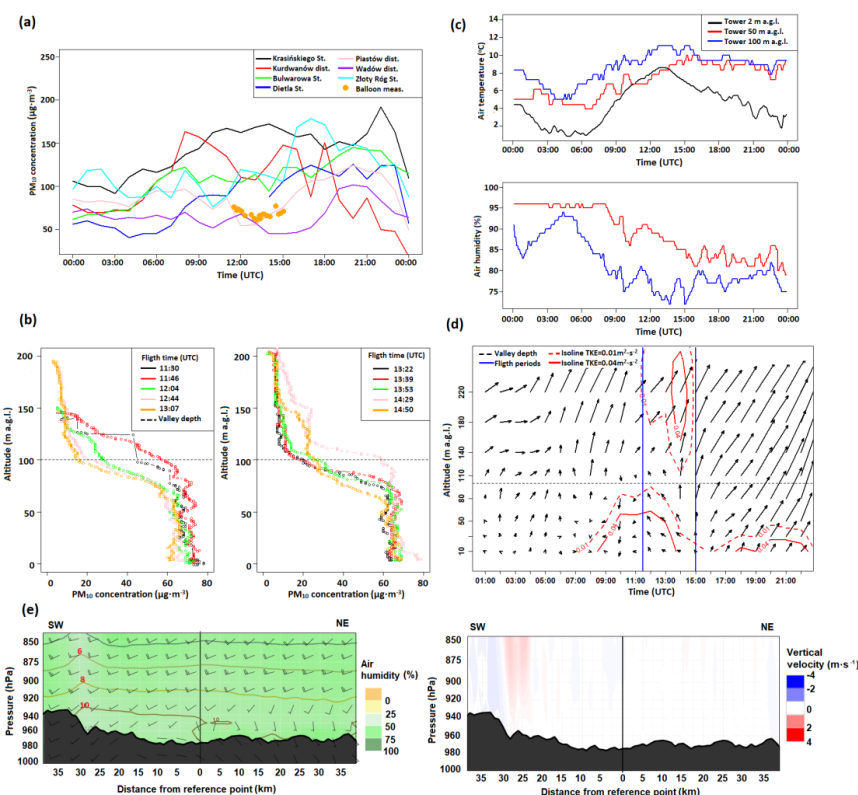
512 *Figure 6. Boxplots of observed height of lower transition layer and predicted height of the convection layer (a),*
513 *the wind shear (c), convection layer and wind shear occurrence occurred at the same model level and summary*
514 *of total cases (d). At figures are included sample size.*
515

516 The results presented in Figure 6 indicate that the median for all cases of the altitude of the lower transition layer
517 oscillates around the valley depth (100 m a.g.l.). The lowest interquartile range of observations is linked with cases
518 where the dominant factor is the height of convection layer (and the presence of wind shear) (Fig. 6 a and c). The
519 predicted height of the lower transition layer was the most consistent with the observations for cases where
520 convection and wind shear occurred at the same vertical model level. For cases where convection height was the
521 dominant factor, the first quartile is too low and for wind shear the position of the upper quartile and the median
522 is too low in comparison with the observations.

523 Data of 28 Nov., 2019, were used as an example of profile type III. Vertical profiles of air humidity and air
524 temperature from model forecast and measurements from TV tower indicated the presence of a persistent ground
525 thermal inversion intensified by warm and dry air advection from the south-west (Fig. 7 c-d). The height of the
526 transition layer did not exceed valley top, and the differences between the individual vertical PM₁₀ concentration
527 profiles were not significant. The height of the transition layer was mostly determined by the height of the
528 convection layer; wind vertical profiles indicated the occurrence of wind shear above the convection layer. The
529 limited range of the convection layer at 28 Nov., 2019, was the result of high cloudiness during the daytime. On
530 that day, foehn conditions were not met at Kasprowy Wierch and Balice station, however the cross section of



531 AROME CMC 1km model indicated the occurrence of foehn in the south-west Western Carpathians. This
532 phenomenon could partially contribute to the warm air advection from south-west. Additionally, data from the air
533 pollution measurement stations showed significant spatial variability of PM_{10} concentration in Kraków. Maximum
534 hourly PM_{10} concentration difference between measurement points was equal to $170 \mu\text{g}\cdot\text{m}^{-3}$. Ground
535 measurements at balloon site were similar to those from Piastów dist., and differences between balloon site and
536 Krasieńskiego St. were in the range from 89 to $107 \mu\text{g}\cdot\text{m}^{-3}$.
537 Similar situations, with significant wind direction change in the vertical profile and weak wind speed, were
538 presented at e.g. Vergeiner, 2004, Li X. et al., 2012 and Li et al. 2015, for mountain valleys, during hydraulic jump
539 occurrence. In the upper layer, wind direction is constant while wind speed increases with height.



540

541 *Figure 7. Hourly concentration at air pollution stations at 28 Nov. 2019 with added ground balloon measurements*
542 *(a) and vertical profiles of PM_{10} concentration (b), vertical profiles of air temperature (c), wind profile forecast*
543 *with added isolines of TKE equal $0.01\text{m}^2\cdot\text{s}^{-2}$ and $0.04\text{m}^2\cdot\text{s}^{-2}$ for city center with marked measurement campaign*
544 *period by blue vertical lines (d) and air humidity at 2 levels from TV tower and (e) SW-NE cross section for city*
545 *center of air temperature (contour lines), air humidity (background), and wind speed (in knots) and direction*
546 *(graphical symbols), and vertical velocity, at 12 UTC 28 Nov. 2019.*

547 *Explanation: valley depth is the altitude of the hilltops surrounding the valley marked at 100 m a.g.l. with a dashed*
548 *line in fig. b and d.*

549

550



551 **5 Discussion**

552 Studies presenting complex thermal structure of boundary layer (e.g. Xu et al. 2019; Wang et al. 2018) indicate
553 that local pollutants are mostly trapped in the lowest layer. The occurrence of multi-layer vertical structure in the
554 boundary layer were noticed during the foehn periods, too, where warm air advection caused the intensification of
555 the air temperature inversion and CAP, and reduction of the available air volume for mixing the pollutants (e.g.
556 sandwich foehn occurrence: Li X. et al., 2015; Vergeiner, 2004). In the present paper, for the days with balloon
557 flights, the occurrence of PM₁₀ profile type III was connected with the advection of air masses from the south.
558 Such advection direction may be linked to the foehn wind occurrence in the Tatra Mts. Therefore, it was checked
559 whether such advection is linked to high PM₁₀ concentration differences between the measurement points within
560 the city, especially between the western, narrow part of the valley and the eastern, wide part. For both cold seasons,
561 cases of PM₁₀ concentration differences > 50 µg m⁻³ which lasted at least for 5 hours constituted 10.9% of the
562 study period. For half of the cases, the dominating wind direction noted in Libertów was from the sector 130-270°.
563 In both cold seasons, wind direction from the sector 130-270° was noted in 52.6% of cases, which shows that it is
564 an important factor controlling PM₁₀ spatial patterns, but the impact is diversified.

565 Research presenting impact of PBL dynamics, confirms that during convective conditions (mechanical and thermal
566 turbulence) vertical distribution of PM concentrations is uniform (Li et al. 2019; Strbova et al., 2017; Wang et al.
567 2018). Mechanical turbulence can be caused by strong wind shear connected to LLJ (Li et al. 2019), mountain
568 waves (Zangl, 2003), hydraulic jump (Kishcha et al. 2017), rotors (Kunin et al. 2019) or passage of an atmospheric
569 front. In the present study, wind shear turned out to be the most important factor in terms of PM₁₀ vertical profile
570 modification. In the case of the study area under investigation, the wind shear is generated due to the relief impact,
571 i.e. the presence of a large valley, blocked on one side with the hills. Studies presented in Sheridan (2019), indicate
572 that the valley width is an important parameter affecting the interactions between CAP and air flow above the
573 valley. For valleys which depth exceeds the depth-scale of the nocturnal stable boundary layer, processes related
574 to daytime insolation may be not strong enough to break the cold-air pool.

575 The data used included both measurement and model data which allowed to verify, as much as possible, the
576 numerical weather predictions. Prognosis of e.g. wind field and TKE is highly dependent on the inclusion of
577 various topographical features in the model formula. Local-scale phenomena like low level jet, cold pool
578 occurrence, and katabatic flows are often under-represented in the model analysis, so the verification with
579 observations is needed.

580 The meteorological and PM₁₀ data for the study periods were compared to the data for the whole two cold seasons
581 and it was found out that they are representative for the situations with very low wind speed and higher than usual
582 air pollution. Therefore, the analyses' outcomes are valid for those periods within the cold season when the
583 aerosanitary conditions are the worst. Additionally, the results obtained may be considered as representative for
584 cities located in large river valleys of Central Europe and applied in the studies concerning the air quality there.

585 **6 Conclusion**

586 The results of our study present how the wind shear generated in a local scale by the diversified relief's impact
587 can be a factor which might significantly modify the spatial pattern of PM₁₀ concentration. We focused mainly on



588 the events characterized by high surface-level PM₁₀ concentrations in the city centre, as such situations are the
589 most dangerous and the most important from the point of view of the inhabitants' health. High PM₁₀ concentrations
590 are usually linked to low wind speed occurrence, and all PM₁₀ concentration vertical profiles were obtained in such
591 conditions, due to safety regulations concerning the balloon operation. The flights' height depended on the height
592 at which the wind speed was too high to continue the uplift. Vertical profiles of PM₁₀ concentration are also
593 strongly dependent on the thickness of the convective layer. We have distinguished three main types of PM₁₀
594 concentration vertical profiles, with type II being the least numerous and observed sporadically, usually as an
595 intermediate short-term form occurring during the development of either type I, or type III. In fact, the air layer
596 inside the valley with constant high PM₁₀ values of vertical concentrations described as type I, was usually found
597 to be only a lowermost section of type III, but the whole profile could not be observed as the wind speed at higher
598 levels was too high to continue the flight. Type III presents the situation where the impact of the wind shear on
599 PM₁₀ concentration profile is not linked mainly to the change in wind speed, like in type I, but to the change in
600 wind direction; the wind speed had to remain low within the whole profile as otherwise the balloon flight could
601 not be realized. In type III, the sudden decrease in PM₁₀ concentrations above the layer with its high constant
602 values are due to the advection of different air masses in a regional scale. The analysis of PM₁₀ profiles from all
603 flights allows to distinguish three vertical zones of potential air pollution hazard within the valley (about 100 m
604 deep) and the city of Kraków:

- 605 1. up to about 60 m a.g.l. – the zone where during periods of low wind speed, air pollution is potentially the
606 highest and the duration of such high levels is the longest, i.e. the zone with the worst aerosanitary
607 conditions;
- 608 2. about 60-100 m a.g.l. – transitional zone where the large decrease of PM₁₀ levels with height is observed;
- 609 3. above 100-120 m a.g.l. – the zone where air quality is significantly better than in the zone 1, either due
610 to the increase of the wind speed, or due to the wind direction change and advection of different, clean
611 air masses

612 Further research is planned, including night balloon measurements during high PM₁₀ concentration episodes.
613 Additionally, it is planned to determine the share of particles of various size fractions in the air pollution with the
614 sensors where light scattering method is applied.

615
616
617
618
619
620
621
622
623
624
625
626
627
628
629
630



631

APPENDICIES

632 *Table A1. Height of the lowest 87 model vertical levels (v.l.) up to 3 km of altitude, used in forecast.*

No. of v.l.	Height of v.l. (km a.g.l.)	No. of v.l. (cont.)	Height of v.l. (km a.g.l.)
1	0.009	20	0.969
2	0.030	21	1.055
3	0.053	22	1.144
4	0.079	23	1.237
5	0.110	24	1.334
6	0.143	25	1.435
7	0.180	26	1.537
8	0.221	27	1.640
9	0.264	28	1.744
10	0.311	29	1.849
11	0.362	30	1.957
12	0.415	31	2.066
13	0.472	32	2.178
14	0.533	33	2.292
15	0.597	34	2.408
16	0.664	35	2.527
17	0.735	36	2.649
18	0.809	37	2.773
19	0.887	38	2.900

633

634

635

636

637

638

639

640

641

642

643

644

645

646

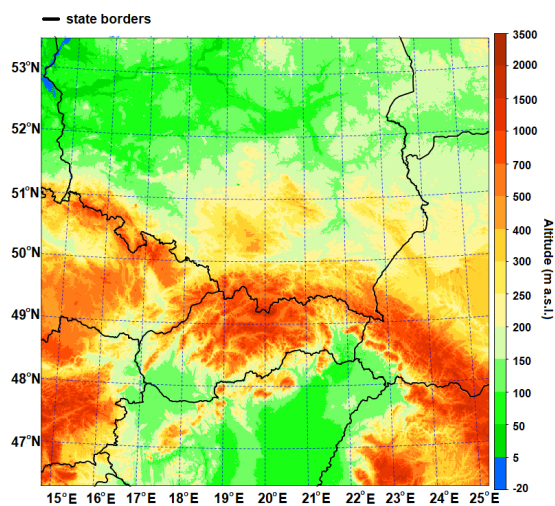


647 *Table A2. Physics schemes used in AROME CMC 1 km model.*

Dynamics	Nonhydrostatic ALADIN (Benard et al., 2010)
Turbulence	Prognostic turbulent kinetic energy (TKE) combined with diagnostic mixing length (Cuxart et al., 2000; Bougeault and Lacarrere, 1989)
Radiation	Longwave Rapid Radiative Transfer Model (RRTM) radiation scheme, Morcrette shortwave radiation scheme from European Centre for Medium-Range Weather Forecasts (ECMWF)
Microphysics	Three-class parameterization (ICE3)
Shallow convection	Pergaud, J., Masson, V., Malardel, S., and Couvreux, F., 2009 (PMMC09) (Pergaud et al., 2009)
Deep Convection	-
Clouds	Statistical cloud scheme
Surface scheme	SURFEX (Masson et al., 2013)

648

649 *Figure A1. Orography map of AROME model domain with resolution 1 km x 1 km.*



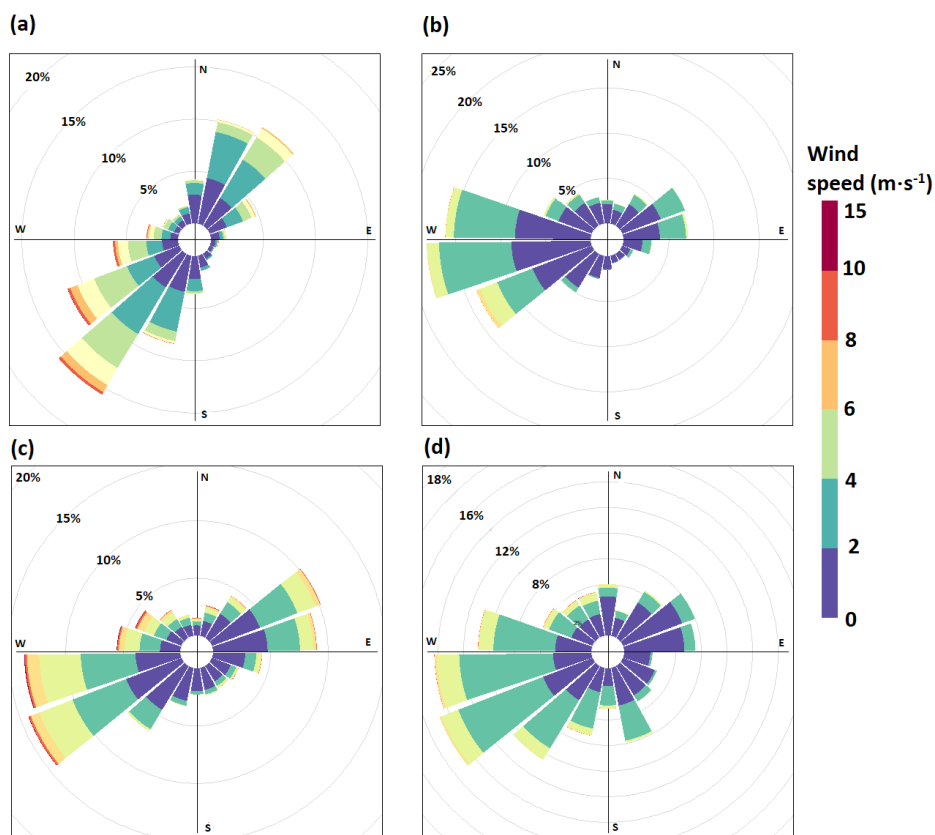
650

651

652



653 *Figure A2. Wind rose for three stations located in the valley Balice (a), Reymonta St.(b), Igołomia (c) and one at*
654 *the nearest hilltop station Libertów (d) for cold seasons 2018-2020.*

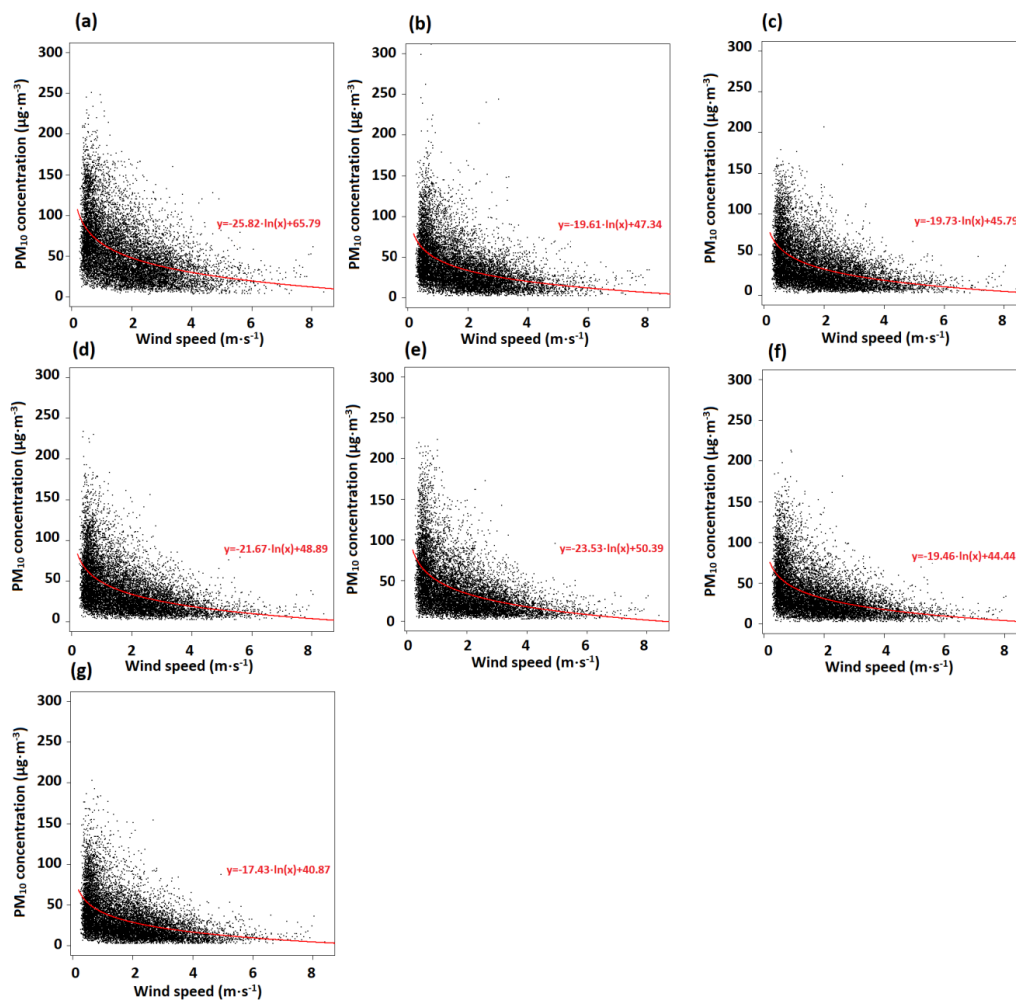


655

656



657 Figure A3. Analysis of hourly PM₁₀ concentration at air pollution stations in Kraków compared to wind speed
658 from Reymonta St. station: a) Krasinkiego St., b) Dietla St., c) Bulwarowa St., d) Złoty Róg St., e) Kurdwanów
659 dist., f) Piastów dist., g) Wadów dist. To presented data is fitted logarithmic curve, at right corner is included
660 curve equation.



661
662
663
664



665

666

667 *Table A3. Distribution of the temperature gradient between levels 200 and 50 m a.g.l. depending on the wind*
 668 *speed at a height of 50 m a.g.l. for city center at two cold seasons 2018-2020 obtained from AROME model*
 669 *forecast.*

		Wind speed range at 50 m a.g.l. [$\text{m}\cdot\text{s}^{-1}$]					
		[0;2)	[2;4)	[4;6)	[6;8)	[8;10)	[10;20)
Air temperature gradient range between layers 200 and 50 m a.g.l. [$^{\circ}\text{C}/100\text{m}$]	[-1.5;-1.0)	371	649	689	437	171	61
	[-1.0;-0.5)	404	965	1065	900	352	171
	[-0.5;0)	244	634	429	145	23	4
	[0;0.5)	306	625	283	41	3	0
	[0.5;1)	322	445	112	6	1	0
	[1;1.5)	303	309	65	4	2	0
	[1.5;2)	193	190	34	7	0	0
	[2;5)	266	316	53	5	2	0
	[5;10)	2	31	0	0	0	0

670

671

672

673

674

675

676

677

678

679

680

681

682

683

684

685

686

687



688 Table A4. List of measurement campaign with specified PM₁₀ profile observed during selected day.

	Type I	Type II	Type III
No.	26 days (10 days with PM ₁₀ maximum concentration above 50µg·m ⁻³ , marked with text in bold)	7 days	13 days
1			28.11.2019
2	01.12.2019		
3	05.12.2019		
4	06.12.2019		
5	09.12.2019		
6	11.12.2019		
7			12.12.2019
8	13.12.2019		
9		17.12.2019	17.12.2019
10	19.12.2019		19.12.2019
11	21.12.2019		
12	22.12.2019		
13	02.01.2020	02.01.2020	02.01.2020
14	03.01.2020	03.01.2020	
15	06.01.2020		
16	07.01.2020		07.01.2020
17	09.01.2020		09.01.2020
18	12.01.2020		
19	13.01.2020		
20			14.01.2020
21	16.01.2020		16.01.2020
22	20.01.2020		
23	25.01.2020		
24	26.01.2020		26.01.2020
25	27.01.2020	27.01.2020	27.01.2020
26		28.01.2020	
27	15.02.2020	15.02.2020	15.02.2020
28	17.02.2020		
29	20.02.2020	20.02.2020	20.02.2020
30	01.03.2020		
31	03.03.2020		

689
 690
 691
 692
 693
 694



695 Code availability: not applicable
696 Data availability: not applicable
697 Author contribution: Piotr Sekuła: Conceptualization, Methodology, Validation, Formal analysis, Visualization,
698 Writing - Original Draft, Writing - Review & Editing, Anita Bokwa: Conceptualization, Methodology, Formal
699 analysis, Writing - Original Draft, Writing - Review & Editing, Jakub Bartyzel: Conceptualization,
700 Methodology, Investigation, Writing - Review & Editing, Bogdan Bochenek: Conceptualization, Writing -
701 Original Draft, Łukasz Chmura: Conceptualization, Investigation, Resources, Writing - Review & Editing,
702 Michał Galkowski: Conceptualization, Investigation, Resources, Writing - Review & Editing, Writing - Review
703 & Editing, Mirosław Zimnoch: Conceptualization, Methodology, Investigation, Writing - Original Draft, Writing
704 - Review & Editing
705 Competing interests: The authors declare that they have no conflict of interest
706
707 **Acknowledgements:** The authors wish to thank Balon Widokowy sp. z o.o. for providing a tethered balloon for
708 the measurement of PM₁₀ vertical profiles in Kraków. This research was partly funded by the EU Project
709 POWR.03.02.00-00-I004/16 (PS) and Ministry of Science and Higher Education subsidy, project no.
710 16.16.220.842-B02.
711
712 **References**
713 Air quality in Europe – 2020 report, 2020, European Environmental Agency. Available online:
714 <https://www.eea.europa.eu/publications/air-quality-in-europe-2020-report>
715
716 Benard, P., Vivoda, J., Masek, J., Smolikova, P., Yessad, K., Smith, C., Brozkova, R., and Geleyn, J. F.:
717 Dynamical kernel of the Aladin-NH spectral limited-area model: Revised formulation and sensitivity
718 experiments, *Quarterly Journal of the Royal Meteorological Society*, 136, 155-169, 10.1002/qj.522, 2010.
719
720 Bochenek, B. Sekuła, P., Jerczyński, M., Kolonko, M., Szczęch-Gajewska, M., Woyciechowska, J., Stachura, G.
721 "ALADIN in Poland", 30th ALADIN Wk & HIRLAM ASM 2020, Ljubljana, Slovenia, 30 March – 3 April
722 2020, http://www.umr-cnrm.fr/aladin/IMG/pdf/poster_poland.pdf
723
724 Bokwa, A.: Miejska wyspa ciepła na tle naturalnego zróżnicowania termicznego obszaru położonego we
725 wklęsłej formie terenu (na przykładzie Krakowa) [Urban heat island against the background of natural thermal
726 diversity of the area located in a concave terrain (on the example of Kraków city)], *Prace Geograficzne IGiGP*
727 *UJ*, 122, 111-132, 2009.
728
729 Bokwa, A.: Wieloletnie zmiany struktury mezoklimatu miasta na przykładzie Krakowa [Long-term changes in
730 the structure mesoclimate of the city on the example of Kraków city], *IGiGP UJ*, Kraków, 296 pp., 2010.
731
732 Bougeault, P., and Lacarrere, P.: PARAMETERIZATION OF OROGRAPHY-INDUCED TURBULENCE IN A
733 MESOBETA-SCALE MODEL, *Monthly Weather Review*, 117, 1872-1890, 10.1175/1520-
734 0493(1989)117<1872:pooiti>2.0.co;2, 1989.



735
736 Cuxart, J., Bougeault, P., and Redelsperger, J. L.: A turbulence scheme allowing for mesoscale and large-eddy
737 simulations, *Quarterly Journal of the Royal Meteorological Society*, 126, 1-30, 10.1002/qj.49712656202, 2000.
738
739 Drechsel S., and Mayr G. J.: Objective Forecasting of Foehn Winds for a Subgrid-Scale Alpine Valley, *Weather
740 and Forecasting*, 23, 205-218, <https://doi.org/10.1175/2007WAF2006021.1>, 2008.
741
742 Fedorovich, E., and Conzemius, R.: Effects of wind shear on the atmospheric convective boundary layer
743 structure and evolution, *Acta Geophysica*, 56, 114-141, 10.2478/s11600-007-0040-4, 2008.
744
745 Ferrero, L., Riccio, A., Ferrini, B. S., D'Angelo, L., Rovelli, G., Casati, M., Angelini, F., Barnaba, F., Gobbi, G.
746 P., Cataldi, M., and Bolzacchini, E.: Satellite AOD conversion into ground PM₁₀, PM_{2.5} and PM₁ over the Po
747 valley (Milan, Italy) exploiting information on aerosol vertical profiles, chemistry, hygroscopicity and
748 meteorology, *Atmospheric Pollution Research*, 10, 1895-1912, 10.1016/j.apr.2019.08.003, 2019.
749
750 Franchini, M., and Mannucci, P. M.: Short-term effects of air pollution on cardiovascular diseases: outcomes and
751 mechanisms, *Journal of Thrombosis and Haemostasis*, 5, 2169-2174, 10.1111/j.1538-7836.2007.02750.x, 2007.
752
753 Franchini, M., and Mannucci, P. M.: Thrombogenicity and cardiovascular effects of ambient air pollution,
754 *Blood*, 118, 2405-2412, 10.1182/blood-2011-04-343111, 2011.
755
756 Giovannini, L., Ferrero, E., Karl, T., Rotach, M. W., Staquet, C., Castelli, S. T., and Zardi, D.: Atmospheric
757 Pollutant Dispersion over Complex Terrain: Challenges and Needs for Improving Air Quality Measurements and
758 Modeling, *Atmosphere*, 11, 32, 10.3390/atmos11060646, 2020.
759
760 Godłowska, J.: Wpływ warunków meteorologicznych na jakość powietrza w Krakowie. Badania porównawcze i
761 próba podejścia modelowego [Influence of meteorological conditions on air quality in Kraków city. Comparative
762 research and an attempt at a model approach], IMGW-PIB, Warszawa, 2019.
763
764 Godłowska, J., Hajto M. J., Tomaszewska A.M., 2015, Spatial analysis of air masses backward trajectories in
765 order to identify distant sources of fine particulate matter emission, *Archives of Environmental Protection*, Vol.
766 41 no. 2 pp. 28–35, DOI 10.1515/aep-2015-0015
767
768 Han, S. Q., Hao, T. Y., Zhang, Y. F., Liu, J. L., Li, P. Y., Cai, Z. Y., Zhang, M., Wang, Q. L., and Zhang, H.:
769 Vertical observation and analysis on rapid formation and evolutionary mechanisms of a prolonged haze episode
770 over central-eastern China, *Science of the Total Environment*, 616, 135-146, 10.1016/j.scitotenv.2017.10.278,
771 2018.
772
773 Hess, M.: *Klimat Krakowa* [Climate of Kraków], *Folia Geogr., ser. Geogr.-Phys.*, 8, 45-102, 1974.
774



- 775 Jeong, S. J.: The Impact of Air Pollution on Human Health in Suwon City, *Asian Journal of Atmospheric*
776 *Environment*, 7-4, 227-233, 10.5572/ajae.2013.7.4.227, 2013.
- 777
- 778 Kishcha, P., Starobinets, B., and Alpert, P.: Modelling of foehn-induced extreme local dust pollution in the Dead
779 Sea valley, in: *Air Pollution Modeling and its Applications XXV*, edited by Mensink, C., and Kallos, G.,
780 Springer Proceedings in Complexity, Springer, Cham., 433–437, DOI 10.1007/978-3-319-57645-9_68, 2017
- 781 Kraków, S. O. i.: *Statistical yearbook of Kraków 2019*, 2019.
- 782
- 783 Kunin, P., Alpert, P., and Rostkier-Edelstein, D.: Investigation of sea-breeze/foehn in the Dead Sea valley
784 employing high resolution WRF and observations, *Atmos. Res.*, 229, 240-254, 10.1016/j.atmosres.2019.06.012,
785 2019.
- 786
- 787 Li, J. W., and Han, Z. W.: Aerosol vertical distribution over east China from RIEMS-Chem simulation in
788 comparison with CALIPSO measurements, *Atmospheric Environment*, 143, 177-189,
789 10.1016/j.atmosenv.2016.08.045, 2016.
- 790
- 791 Li, X., Xia, X. G., Xin, Y., Ma, Y. F., Yang, J., Li, J. L., and Yang, X. H.: An examination of boundary layer
792 structure under the influence of the gap winds in Urumqi, China, during air pollution episode in winter, *Journal*
793 *of the Air & Waste Management Association*, 62, 26-37, 10.1080/10473289.2011.617628, 2012.
- 794
- 795 Li, X., Xia, X., Wang, L., Cai, R., Zhao, L., Feng, Z., Ren, Q., and Zhao, K.: The role of foehn in the formation
796 of heavy air pollution events in Urumqi, China, *Journal of Geophysical Research-Atmospheres*, 120, 5371-5384,
797 10.1002/2014jd022778, 2015.
- 798
- 799 Li, X. L., Ma, Y. J., Wei, W., Zhang, Y. H., Liu, N. W., Hong, Y., and Wang, Y.: Vertical Distribution of
800 Particulate Matter and its Relationship with Planetary Boundary Layer Structure in Shenyang, Northeast China,
801 *Aerosol and Air Quality Research*, 19, 2464-2476, 10.4209/aaqr.2019.06.0311, 2019.
- 802
- 803 Liu, C., Huang, J. P., Wang, Y. W., Tao, X. Y., Hu, C., Deng, L. C., Xu, J. P., Xiao, H. W., Luo, L., Xiao, H. Y.,
804 and Xiao, W.: Vertical distribution of PM_{2.5} and interactions with the atmospheric boundary layer during the
805 development stage of a heavy haze pollution event, *Science of the Total Environment*, 704,
806 10.1016/j.scitotenv.2019.135329, 2020.
- 807
- 808 Marynowski, L., Łupikasza, E., Dąbrowska-Zapart, K., Małarzewski, Ł., Niedźwiedź, T., and Simoneit, B. R. T.:
809 Seasonal and vertical variability of saccharides and other organic tracers of PM₁₀ in relation to weather
810 conditions in an urban environment of Upper Silesia, Poland, *Atmospheric Environment*, 242, 117849,
811 10.1016/j.atmosenv.2020.117849, 2020.
- 812
- 813 Masson, V., Le Moigne, P., Martin, E., Faroux, S., Alias, A., Alkama, R., Belamari, S., Barbu, A., Boone, A.,
814 Bouyssel, F., Brousseau, P., Brun, E., Calvet, J. C., Carrer, D., Decharme, B., Delire, C., Donier, S., Essaoui,



815 K., Gibelin, A. L., Giordani, H., Habets, F., Jidane, M., Kerdraon, G., Kourzeneva, E., Lafaysse, M., Lafont, S.,
816 Brossier, C. L., Lemonsu, A., Mahfouf, J. F., Marguinaud, P., Mokhtari, M., Morin, S., Pigeon, G., Salgado, R.,
817 Seity, Y., Taillefer, F., Tanguy, G., Tulet, P., Vincendon, B., Vionnet, V., and Voldoire, A.: The SURFEXv7.2
818 land and ocean surface platform for coupled or offline simulation of earth surface variables and fluxes,
819 *Geoscientific Model Development*, 6, 929-960, 10.5194/gmd-6-929-2013, 2013.

820

821 Pergaud, J., Masson, V., Malardel, S., and Couvreux, F.: A Parameterization of Dry Thermals and Shallow
822 Cumuli for Mesoscale Numerical Weather Prediction, *Boundary-Layer Meteorology*, 132, 83-106,
823 10.1007/s10546-009-9388-0, 2009.

824

825 PM10 emissions in the European Union (EU-28) in 2018, 2021, Statista (www.statista.com), Last access: 6 Jan.,
826 2021: [https://www.statista.com/statistics/879414/pm10-particulate-matter-emission-contributions-european-](https://www.statista.com/statistics/879414/pm10-particulate-matter-emission-contributions-european-union-eu-28/)
827 [union-eu-28/](https://www.statista.com/statistics/879414/pm10-particulate-matter-emission-contributions-european-union-eu-28/)

828

829 Raport o stanie środowiska w województwie małopolskim w 2017 roku [Report about the state of the
830 environment in the Małopolska Voivodeship in 2017], 2017, Voivodeship Inspectorate of Environmental
831 Protection, Kraków (in Polish). Available at:
832 <http://www.krakow.pios.gov.pl/Press/publikacje/raporty/raport17/raport2017.pdf>

833

834 Roczna ocena jakości powietrza w województwie Małopolskim. Raport wojewódzki za rok 2019 [Annual
835 assessment of air quality in Lesser Poland region. Report for the year 2019], 2020, Chief Inspectorate of
836 Environmental Protection, Kraków (in Polish). Available at:
837 <https://powietrze.gios.gov.pl/pjp/rwms/publications/card/1163>

838

839

840 Renard, J. B., Michoud, V., and Giacomoni, J.: Vertical Profiles of Pollution Particle Concentrations in the
841 Boundary Layer above Paris (France) from the Optical Aerosol Counter LOAC Onboard a Touristic Balloon,
842 *Sensors*, 20, 10.3390/s20041111, 2020.

843

844 Rodier, Q., Masson, V., Couvreux, F., and Paci, A.: Evaluation of a Buoyancy and Shear Based Mixing Length
845 for a Turbulence Scheme, *Frontiers in Earth Science*, 5, 17, 10.3389/feart.2017.00065, 2017.

846

847 Samad, A., Vogt, U., Panta, A., and Uprety, D.: Vertical distribution of particulate matter, black carbon and
848 ultra-fine particles in Stuttgart, Germany, *Atmospheric Pollution Research*, 11, 1441-1450,
849 10.1016/j.apr.2020.05.017, 2020.

850

851 Sheridan P.F.: Synoptic-flow interaction with valley cold-air pools and effects on cold-air pool persistence:
852 Influence of valley size and atmospheric stability, *Q. J. R. Meteorol. Soc.*, 145, 1636-1659,
853 <https://doi.org/10.1002/qj.3517>, 2019.

854



- 855 Strbova, K., Raclavska, H., and Bilek, J.: Impact of fugitive sources and meteorological parameters on vertical
856 distribution of particulate matter over the industrial agglomeration, *Journal of Environmental Management*, 203,
857 1190-1198, 10.1016/j.jenvman.2017.06.001, 2017.
- 858
- 859 Termonia, P., Fischer, C., Bazile, E., Bouyssel, F., Brozkova, R., Benard, P., Bochenek, B., Degrauwe, D.,
860 Derkova, M., El Khatib, R., Hamdi, R., Masek, J., Pottier, P., Pristov, N., Seity, Y., Smolikova, P., Spaniel, O.,
861 Tudor, M., Wang, Y., Wittmann, C., and Joly, A.: The ALADIN System and its canonical model configurations
862 AROME CY41T1 and ALARO CY40T1, *Geoscientific Model Development*, 11, 257-281, 10.5194/gmd-11-
863 257-2018, 2018.
- 864
- 865 Thürkow, M., Kirchner, I., Kranenburg, R., Timmermans, R. M. A., and Schaap, M.: A multi-meteorological
866 comparison for episodes of PM10 concentrations in the Berlin agglomeration area in Germany with the LOTOS-
867 EUROS CTM, *Atmospheric Environment*, 244, 117946, 10.1016/j.atmosenv.2020.117946, 2021.
- 868
- 869 Trompetter, W. J., Grange, S. K., Davy, P. K., and Ancelet, T.: Vertical and temporal variations of black carbon
870 in New Zealand urban areas during winter, *Atmospheric Environment*, 75, 179-187,
871 10.1016/j.atmosenv.2013.04.036, 2013.
- 872
- 873 Ustrnul, Z.: Influence of foehn winds on air-temperature and humidity in the Polish Carpathians, *Theoretical and*
874 *Applied Climatology*, 45, 43-47, 10.1007/bf00865992, 1992.
- 875
- 876 Vergeiner, J.: South foehn studies and a new foehn classification scheme in the Wipp and Inn valley, Ph.D.
877 thesis, Univ. of Innsbruck, Austria, 2004.
- 878
- 879 Wang, D. X., Stachlewska, I. S., Song, X. Q., Heese, B., and Nemuc, A.: Variability of the Boundary Layer Over
880 an Urban Continental Site Based on 10 Years of Active Remote Sensing Observations in Warsaw, *Remote*
881 *Sensing*, 12, 33, 10.3390/rs12020340, 2020.
- 882
- 883 Wang, H., Sun, Z. B., Li, H. Y., Gao, Y., Wu, J., and Cheng, T. T.: Vertical-distribution Characteristics of
884 Atmospheric Aerosols under Different Thermodynamic Conditions in Beijing, *Aerosol and Air Quality*
885 *Research*, 18, 2775-2787, 10.4209/aaqr.2018.03.0078, 2018.
- 886
- 887
- 888 Xu, Y. W., Zhu, B., Shi, S. S., and Huang, Y.: Two Inversion Layers and Their Impacts on PM2.5 Concentration
889 over the Yangtze River Delta, China, *Journal of Applied Meteorology and Climatology*, 58, 2349-2362,
890 10.1175/jamc-d-19-0008.1, 2019.
- 891
- 892 Zängl, G.: Deep and shallow south foehn in the region of Innsbruck: Typical features and semi-idelized
893 numerical simulations. *Meteorol. Atmos. Phys.*, 83, 237-261, <https://doi.org/10.1007/s00703-002-0565-7>, 2003.
- 894



- 895 Zhang, H. L., Wang, Y. G., Hu, J. L., Ying, Q., and Hu, X. M.: Relationships between meteorological
896 parameters and criteria air pollutants in three megacities in China, *Environmental Research*, 140, 242-254,
897 10.1016/j.envres.2015.04.004, 2015.
898
- 899 Zhang, K., Wang, D. F., Bian, Q. G., Duan, Y. S., Zhao, M. F., Fei, D. N. A., Xiu, G. L., and Fu, Q. Y.: Tethered
900 balloon-based particle number concentration, and size distribution vertical profiles within the lower troposphere
901 of Shanghai, *Atmospheric Environment*, 154, 141-150, 10.1016/j.atmosenv.2017.01.025, 2017.
902
- 903 Zhao, S. P., Yu, Y., Qin, D. H., Yin, D. Y., Du, Z. H., Li, J. L., Dong, L. X., He, J. J., and Li, P.: Measurements
904 of submicron particles vertical profiles by means of topographic relief in a typical valley city, China,
905 *Atmospheric Environment*, 199, 102-113, 10.1016/j.atmosenv.2018.11.035, 2019.
906
- 907 Zhou, S. Z., Wu, L. L., Guo, J. C., Chen, W. H., Wang, X. M., Zhao, J., Cheng, Y. F., Huang, Z. Z., Zhang, J. P.,
908 Sun, Y. L., Fu, P. Q., Jia, S. G., Tao, J., Chen, Y. N., and Kuang, J. X.: Measurement report: Vertical distribution
909 of atmospheric particulate matter within the urban boundary layer in southern China - size-segregated chemical
910 composition and secondary formation through cloud processing and heterogeneous reactions, *Atmospheric
911 Chemistry and Physics*, 20, 6435-6453, 10.5194/acp-20-6435-2020, 2020.
912